A KECK/LRIS SPATIALLY RESOLVED SPECTROSCOPIC STUDY OF A LINER GALAXY SDSS J091628.05+420818.7

HYUN-JIN BAE[1], JONG-HAK WOO[2], MASAFUMI YAGI[3], SUK-JIN YOON[1], AND MICHITOSHI YOSHIDA[4]
[1] Department of Astronomy and Center for Galaxy Evolution Research, Yonsei University, Seoul 120-749, Republic of Korea
[2] Astronomy Program, Department of Physics and Astronomy, Seoul National University, Seoul 151-742, Republic of Korea; woo@astro.snu.ac.kr
[3] Optical and Infrared Astronomy Division, National Astronomical Observatory of Japan, Tokyo 181-8588, Japan
[4] Hiroshima Astrophysical Science Center, Hiroshima University, Hiroshima 739-8526, Japan

ABSTRACT

Using spatially resolved spectra obtained with the Low Resolution Imaging Spectrometer at the Keck I telescope, we investigate the nature of ionizing sources and kinematic properties of emission-line gas in a LINER galaxy SDSS J091628.05+420818.7, which is a nearby ($z = 0.0241$) and bright ($M_r = -20.2$) early-type galaxy. After subtracting stellar absorption features using a combination of simple stellar population models, we measure the flux, line-of-sight velocity, and velocity dispersion of four emission lines, i.e., Hα, Hβ, [O III] λ5007, and [N II] λ6584, to study radial change of emission-line fluxes and velocities. Compared to the point-spread function of the observation, the emission-line region is slightly extended but comparable to the seeing size. The central concentration of emission-line gas suggests that ionization is triggered by a nuclear source, excluding old stellar population as ionizing sources. We find that emission-line gas is counter-rotating with respect to stellar component and that the [O III] λ5007 line is blueshifted compared to other emission lines, possibly due to an outflow.

Key words: galaxies: active – galaxies: kinematics and dynamics

Online-only material: color figures

1. INTRODUCTION

Active galactic nuclei (AGNs) may play an important role in galaxy evolution by feeding energy to host galaxies, quenching star formation (e.g., Hopkins et al. 2005; Springel et al. 2005), and leading to the black-hole–galaxy-scaling relations as observed in the local universe (Ferrarese & Merritt 2000; Gebhardt et al. 2000; Gültekin et al. 2009; Woo et al. 2010). By including simple AGN feedback prescriptions, recent semi-analytic models successfully reproduced several observed properties including luminosity function, masses, and colors of galaxies (Croton et al. 2006; Bower et al. 2006), although it is still unclear how AGN feedback works in quenching star formation. Observational studies have found that the majority of early-type galaxies exhibit LINER (Low-Ionization Nuclear Emission-line Region; Heckman 1980) features at the central region (e.g., Ho et al. 1997; Annibali et al. 2010; Capetti & Baldi 2011). If LINERs are truly AGNs, the high fraction of LINERs is consistent with the scenario that the AGN feedback works as a star formation quenching mechanism in early-type galaxies.

In spite of the large population of LINERs in the local universe, the nature of ionizing source of LINERs is still debated. On one hand, LINERs have been generally regarded as a branch of low-luminosity AGNs (e.g., Ho et al. 1997; Kauffmann et al. 2003; Kewley et al. 2006). This idea has been supported by several studies on nearby LINER galaxies, which provided much smoking-gun evidence for AGN origin of LINER features, e.g., the presence of broad emission lines (e.g., Ho et al. 1997), compact emission-line region (e.g., Keel 1983; Pogge et al. 2000), and ultraviolet (UV) flux variability (e.g., Maoz et al. 2005).

On the other hand, narrow-line features of LINER (i.e., Type 2 LINER) can be easily produced by other ionizing mechanisms since the LINER features are characterized by strong low-ionization lines, such as [O I], [N II], and [S II], relative to high-ionization and the recombination lines. Several studies suggested possible mechanisms, e.g., evolved old stars, evolved

young stars, and supernova shocks, for producing the LINER-like features (Binette et al. 1994; Dopita & Sutherland 1995; Taniguchi et al. 2000). By using photoionization models, for example, Binette et al. (1994) showed that evolved old stars, i.e., post-asymptotic giant branch (PAGB) stars, can produce Lyman continuum photons and exhibit LINER-like features, suggesting that a large fraction of LINERs among early-type galaxies can be originated by evolved stars (see also Stasińska et al. 2008). However, these models highly depend on the evolutionary tracks of PAGB stars, which are constructed under a number of theoretical assumptions (e.g., Stanghellini & Renzini 2000). By comparing the measured line flux ratios of a sample of nearby galaxies with photoionization model predictions from Binette et al. (1994), Annibali et al. (2010) reported that 11 out of 49 ($\sim$22%) LINER galaxies could be produced by PAGB stars, while the remaining $\sim$78% galaxies required additional ionization mechanisms. Since they adopt the model prediction of Binette et al. (1994), one should again keep in mind the model uncertainties. In a similar way, Taniguchi et al. (2000) suggested young evolved stars, i.e., planetary nebulae, from recent starburst as a viable mechanism for LINER-like features, implying a close connection between post-starburst and LINER-like phenomena. This scenario provides an alternative explanation of LINER features particularly for late-type galaxies. In addition to old and young stars, radiative shocks from oxygen-rich supernova can also produce LINER-like features without an AGN as suggested by Dopita & Sutherland (1995).

In contrast to the spatially concentrated LINER features originated from AGNs (Keel 1983; Pogge et al. 2000), those LINER-like emissions due to non-AGN mechanisms tend to be spatially extended (Veilleux et al. 1995; Monreal-Ibero et al. 2006; Rich et al. 2010; Sarzi et al. 2010). For example, Pogge et al. (2000) investigated the size of narrow-line region (NLR) of 14 LINER galaxies based on the high spatial resolution narrowband imaging data from the *Hubble Space Telescope* and showed that the most of the emission comes from central regions with the size of tens to hundreds of parsecs (pc), indicating that

central AGN activities are responsible for the LINER features. In contrast, Rich et al. (2010) reported extended LINER emission in NGC 839, concluding that the LINER-like feature is related to other mechanisms than an AGN.

It is also possible that LINER-like features observed with limited spatial resolutions may be a mixed bag of various ionization mechanisms (e.g., Filippenko 1996). For nearby ($z <$ 0.01) galaxies, spectroscopic observations generally include nuclear emission from the central ∼100 pc region, avoiding possible contamination from an extended emission-line region. In contrast, it is far more complicated to understand the nature of emission lines in integrated spectra obtained with a large aperture, for example, Sloan Digital Sky Survey (SDSS; York et al. 2000)[5] spectroscopic observations with a 3″ diameter fiber include emissions from much larger physical scale (∼5 kpc) in SDSS galaxies with a mean redshift $z \sim$ 0.1. Hence, it is possible that even non-AGN galaxies can be interpreted as LINER galaxies due to contaminations from extended LINER-like emission region. While a number of studies classified SDSS LINERs as AGNs (e.g., Kauffmann et al. 2003; Kewley et al. 2006), other studies argued that the SDSS LINERs may not be related to AGN activity (e.g., Stasińska et al. 2008; Sarzi et al. 2010; Cid Fernandes et al. 2011; Yan & Blanton 2012). For example, Sarzi et al. (2010) discussed that if SDSS LINER galaxies have modest equivalent width of [O III] λ5007 ($\lesssim$2.4 Å), only a small fraction of these galaxies are truly powered by AGNs. A recent statistical study by Yan & Blanton (2012) further claimed that AGN is not a primary ionizing source in the SDSS LINER galaxies although they cannot rule out the presence of a true AGN hidden in the integrated spectra obtained with a large aperture in SDSS.

Since the SDSS provides one of the largest galaxy samples in the local universe, revealing the true nature of LINERs in the SDSS sample is a crucial step in understanding AGN demography in the local universe, and the nature of the galaxy-AGN coevolution. Spatially resolved spectroscopy can shed light on the nature of ionizing source by constraining whether the emission is from nuclear or extended region. The kinematic information of both stellar component and emission-line region can also provide useful hints on the dynamical relation between emission-line gas and stellar component.

To investigate the true nature of LINER features, we performed a pilot study using a carefully selected LINER early-type galaxy, SDSS J091628.05+420818.7, from SDSS DR7 (Abazajian et al. 2009). In this work, we present detailed analysis on the emission-line properties based on the spatially resolved spectroscopy. The paper is composed as follows. Section 2 describes sample selection, observations, and data reduction. Section 3 presents an analysis method on the extracted spectra. We present the main results on the spatial profile and kinematics of emission lines in Section 4. Finally, we summarize and discuss our findings in Section 5. Throughout the paper, we use ΛCDM cosmological parameters, i.e., $H_o = 70$ km s^{-1} Mpc^{-1}, $\Omega_\Lambda = 0.73$, and $\Omega_m = 0.27$.

2. OBSERVATIONS AND DATA REDUCTION

2.1. Sample Selection

We selected a sample of low-redshift (0.02 $<$ z $<$ 0.05) and bright (r-band absolute magnitude $M_r <$ −19.7) early-type galaxies with LINER features from SDSS DR7 to study

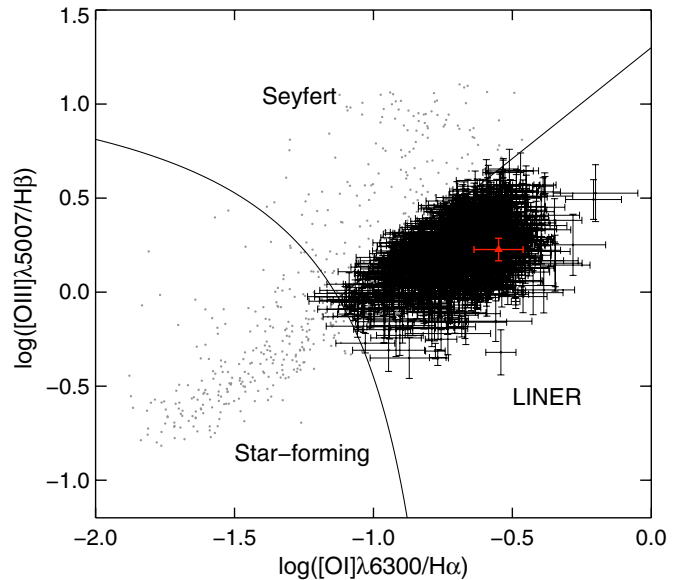**Figure 1.** AGN diagnostic diagram for the LINER early-type galaxies selected from the SDSS. Gray dots represent 1382 nearby (0.02 < z < 0.05) and bright ($M_r <$ −19.7) early-type galaxies with S/N > 3.0 for four emission lines, i.e., Hβ, [O III] λ5007, [O I] λ6300, and Hα. A sample of 902 LINERs (black dots with error bars) are identified by adopting an empirical demarcation line of Kewley et al. (2006) between Seyferts and LINERs. We select a typical LINER early-type galaxies from the LINER sample (red point with error bar). The curved line indicates a theoretical demarcation line between star-forming and AGN-host galaxies (Kewley et al. 2001).

(A color version of this figure is available in the online journal.)

the characteristics of LINER host galaxies (H.-J. Bae et al. in preparation). To represent the general population of LINERs, which are mostly hosted by early-type galaxies, and to avoid contribution from star-forming regions to the observed emission lines, we first selected early-type galaxies based on $u−r$ color and $g−i$ color gradient using the criteria by Park & Choi (2005). Then, LINERs are identified following the criteria of Kewley et al. (2006) on the emission-line ratios (see Figure 1; Baldwin et al. 1981). We used four emission lines retrieved from the MPA-JHU catalog on the SDSS DR7 galaxies,[6] i.e., Hβ, [O III] λ5007, [O I] λ6300, and Hα, with signal-to-noise ratio (S/N) larger than 3.0. To examine whether recent star formation can account for LINER features, we further selected galaxies with the near-UV (NUV)−r color less than 5.5, which is an empirical demarcation line for the early-type galaxies with a recent ($\lesssim$1 Gyr) star formation (Kaviraj et al. 2007).

For a pilot study to constrain the nature of LINER emissions detected in SDSS galaxies, we chose from the sample one galaxy, SDSS J091628.05+420818.7, which represents general characteristics of the LINER early-type galaxies, with $M_r =$ −20.2 and the effective radius of 2.7 kpc. At the redshift of 0.0241, the galaxy provides a reasonable spatial resolution, 0.51 kpc arcsec^{-1}. Figure 1 shows emission-line properties of the sample of SDSS LINER early-type galaxies with $M_r <$ −19.7 and 0.02 < z < 0.05, as well as the selected galaxy.

The galaxy's morphology in the SDSS optical images indicates a lack of recent and/or ongoing merger event (see Figure 2). Spatially extended UV-excess with NUV−r color was measured as 4.9 in the NUV images from *Galaxy Evolution Explorer* (Martin et al. 2005),[7] suggesting that an existence of
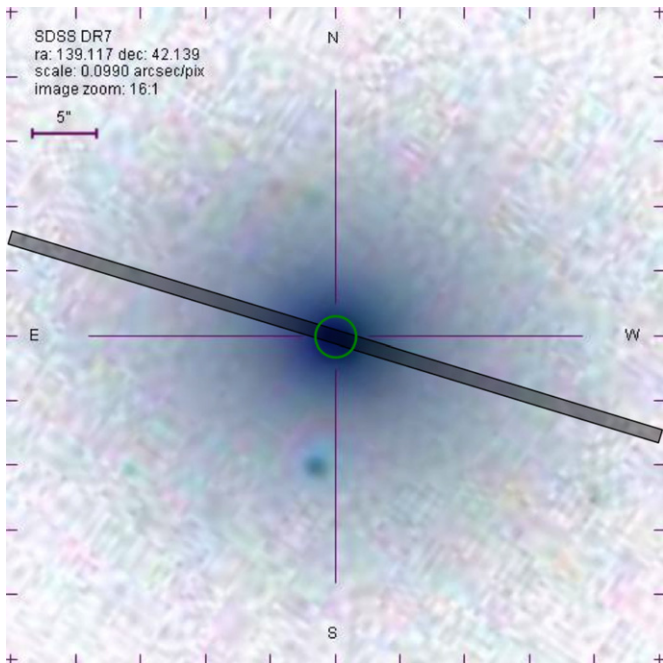
Figure 2. SDSS optical (*gri*) composite color image of the selected LINER early-type galaxy, SDSS J091628.05+420818.7. The angle and the width of the black bar represent the position angle (+73°) and the width (1″) of the slit, respectively. For comparison the 3″ diameter SDSS fiber size is shown at the center (green circle).

(A color version of this figure is available in the online journal.)

spatially extended young stellar population. No radio counterpart for the galaxy is detected at 1.4 GHz through the VLA FIRST survey (Becker et al. 1995).[8]

2.2. Observations

We performed a spatially resolved spectroscopy on the selected target, SDSS J091628.05+420818.7, using the Low Resolution Imaging Spectrometer (LRIS; Oke et al. 1995; Rockosi et al. 2010) at the Keck I telescope with 1 hr (6 × 600 s) exposure on 2011 March 31. The D560 dichroic mirror was used to split the incoming light into the red and blue side CCDs, and the 600/4000 grism and the 600/7500 grating were used for the blue and red sides, respectively. The instrumental setup was chosen to cover the spectral range from 3200 Å to 9000 Å, including forbidden lines [O III] λ5007, [N II] λ6584, and Balmer lines, i.e., Hα, Hβ, which are essential ingredients to identify LINERs. We used a 1″ wide slit with the position angle of +73° counterclockwise direction from the north to the east, which was determined as a major axis based on IRAF/ellipse fitting using the SDSS *g*-band image. To increase S/N, we used 2×2 binning in the CCD, resulting in a spatial scale 0″.27 pixel^{-1}. The dispersion scales for the blue and red sides are 1.23 Å pixel^{-1} and 1.60 Å pixel^{-1}, respectively.

To calibrate the flux and estimate the seeing size, we observed two spectrophotometric stars, Feige 34 and Feige 66 (Oke 1990), right before and after observing the target galaxy. The seeing size decreased during our observations from ∼1″.6 to ∼1″.1 and from ∼1″.2 to ∼0″.9 on the blue and red sides, respectively. The effect of seeing and its variation is discussed in Section 3.3.

8 http://sundog.stsci.edu

2.3. Data Reduction

We reduced the spectroscopic data using a series of IRAF scripts including *twodspec* package as previously performed (e.g., Woo et al. 2006; McGill et al. 2008). The reduction process includes standard procedures, i.e., bias subtraction, flat-fielding, wavelength and flux calibrations. After bias subtraction and flat-fielding, we removed cosmic rays using the Laplacian cosmic-ray identification algorithm (van Dokkum 2001). Arc lines (Hg, Ne, Ar, Cd, and Zn) and sky emission lines were used to calibrate wavelength scales for blue and red sides, respectively. Atmospheric extinction was corrected for each exposure while the galactic extinction was corrected using `deredden` task. Flux calibration was performed using two spectrophotometric standard stars Feige 34 and Feige 66, which were observed with the same instrumental setup during the observing run. After subtracting sky background by adopting sky regions at >20″ from the galaxy center, we extracted nine spectra consecutively along the spatial direction using a 4 pixel aperture diameter, which is equivalent to 1″.08 and ∼0.55 kpc at the distance of the target. However, we only used five central apertures in our analysis, since we could not detect weak emission lines, especially Hβ, from the spectra extracted from the outer region. Thus, we cover the spatial range from −1.1 kpc (SW) to +1.1 kpc (NE) with respect to the center of the galaxy.

Finally, we combined the extracted spectra from each exposure with a median filtering, after scaling fluxes to a mean flux averaged over from 4950 Å to 5150 Å and from 6400 Å to 6800 Å for blue and red sides, respectively. The selected ranges are most preferred since they include useful emission lines for AGN diagnostics, e.g., Hβ and [O III] λ5007 on the blue side, [O I] λ6300, Hα, and [N II] λ6584 on the red side. Using arc and sky emission lines, we measured the instrumental resolutions as 6.1 Å and 4.2 Å FWHM, respectively for blue and red sides, corresponding to Gaussian velocities ∼152 and ∼80 km s^{-1} at the wavelength of the observed Hβ and Hα. The final reduced spectra along the spatial direction are presented in Figure 3.

3. ANALYSIS

In this section, we describe the method for measuring the emission-line fluxes. Since it is crucial to remove stellar absorption features to reliably measure the emission-line fluxes, we first present the procedure for subtracting stellar absorption line (e.g., Ho 2008). Then, we present the emission-line flux measurements. Lastly, we describe how we construct the point-spread function (PSF).

3.1. Stellar Continuum Subtraction

In order to subtract the stellar absorption lines, we need to construct a best-fit stellar model with a combination of stellar templates or population models. Here, we exploit 47 MILES simple stellar population (SSP) templates (Sánchez-Blázquez et al. 2006), which include the population age from 60 Myr to 12.6 Gyr, with twice-solar metallicity ($Z = 0.03$) and the Kroupa initial mass function (Kroupa 2001). For a consistency check we compare the results using SSP models with solar metallicity ($Z = 0.02$), leading to little difference with slightly higher χ^2 value of the fitting.

We construct a best-fit stellar model for galaxy spectra using the penalized pixel-fitting code (pPXF; Cappellari & Emsellem
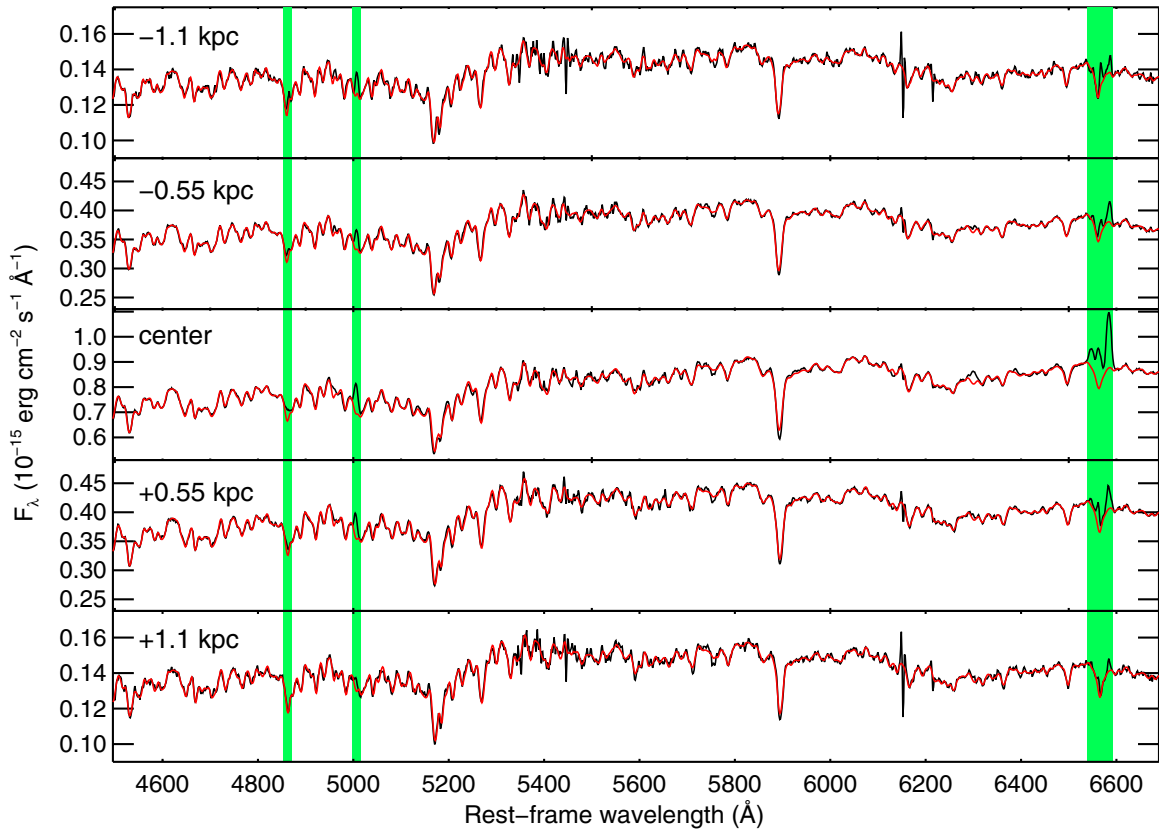
Figure 3. Observed spectra at each aperture along the slit (black line) are plotted over the best-fit stellar models (red line) at each panel. The corresponding distance from the center is denoted in the upper-left corner. The spectral range of each emission line, i.e., Hβ, [O III] λ5007, and Hα+[N II] doublet, is marked with green shades from shorter to longer wavelength, respectively. All spectra are shifted to the rest frame using the velocity measured from the central aperture.

(A color version of this figure is available in the online journal.)

2004),[9] which is widely used in stellar continuum subtraction and gas-kinematics analysis for individual galaxies and large surveys (e.g.. Falcón-Barroso et al. 2004; Cappellari et al. 2011). The pPXF implemented the MPFIT code (Markwardt 2009), which is based on the Levenberg–Marquardt algorithm (Moré 1978) for χ^2 minimization. For the fitting process, we use the limited rest-frame wavelength range from 3550 Å to 7380 Å, to match the available wavelength range of the MILES SSP templates

We mask out the wavelength ranges of well-known nebular emission lines and sky absorption features during the fitting process. To account for imperfect flux calibration and increase the quality of the fit, we adopt a multiplicative polynomial function. Note that we choose a high-order (100–200) polynomial depending on the shape of spectra; however, the polynomial function does not significantly affect the results since the polynomial function does not attempt to fit any single emission line. During this process, we simultaneously measure the first (line-of-sight velocity) and second moments (velocity dispersion) of the stellar absorption lines using spectra obtained at each aperture, which are used to construct the radial profile of rotational velocity and velocity dispersion of stellar component as described in Section 4.2. To measure stellar velocity dispersion, we use the ~200 Å range of spectra including the Mgb triplet and Fe (5270, 5300 Å) lines. We correct for the instrumental resolutions of the observed spectra and the MILES SSP templates (FWHM = 2.51 Å) by subtracting them in quadrature (see Equation (1)

in Woo et al. 2004). The typical measurement errors of stellar velocity dispersion determined from the fitting procedure are ~5%. Using the spectrum extracted from the central aperture, we measure stellar velocity dispersion as 178 ± 10 km s^{-1}, which is consistent with 182 ± 3.8 km s^{-1} measured from the 3″ diameter fiber spectrum of SDSS. In Figure 3, we present the best-fit stellar models overlaid with the observed spectra at each aperture. All spectra are shifted from the observed-frame to the rest-frame using the radial velocity measured from the central aperture.

After the continuum fit, we subtract the stellar model from the observed spectra, revealing the stellar absorption corrected nebular emission lines, which are used in emission-line measurement (see Section 3.2 and Figure 4). The standard deviations of the residuals from stellar subtraction (excluding emission-line regions) are 7.0×10^{-18} erg cm^{-2} s^{-1} Å^{-1} and 1.8×10^{-18} erg cm^{-2} s^{-1} Å^{-1} for apertures at the center and outer (+1.1 kpc), respectively. For comparison, peaks of flux density for each emission line are significantly larger than the residual from stellar subtraction ($>3\sigma$), confirming that the stellar fit is good enough to measure emission-line fluxes. In the case of the Hβ at +1.1 kpc aperture, which is the weakest emission line we measured, the peak of flux density is comparable to the fitting residual, indicating that it is difficult to measure the weak Hβ emission-line flux at +1.1 kpc aperture.

3.2. Emission-line Measurement

After the stellar subtraction, we measure four emission lines for each aperture; Hβ, [O III] λ5007, Hα, and [N II] λ6584. The
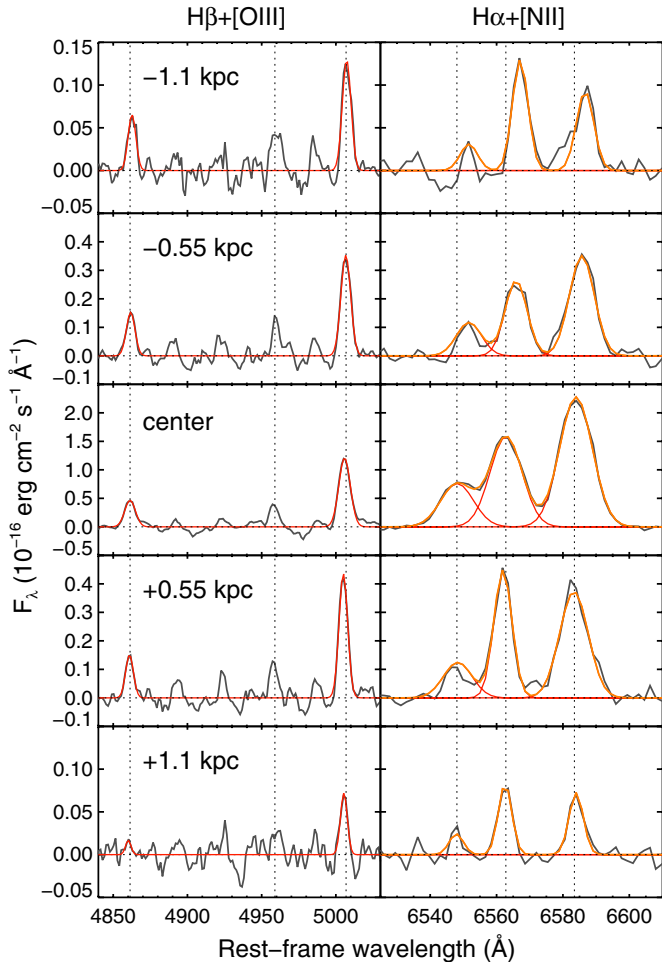
Figure 4. Residual emission lines (gray line) after subtracting stellar continuum and the best-fit emission-line model (red line) for the Hβ+[O III] (left panel) and the Hα+[N II] regions (right panel), respectively. Vertical lines represent the reference wavelength of each emission line. The distance from the center is denoted in left-hand side panels. Orange lines on the right-hand side panels exhibit the sum of three Gaussian functions for Hα and [N II] doublet.

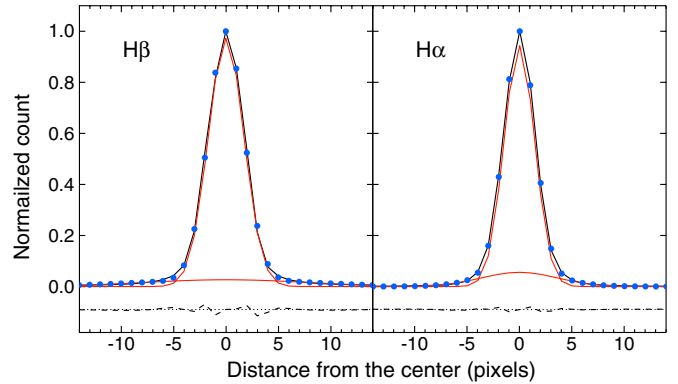(A color version of this figure is available in the online journal.)

Figure 5. PSF models based on the observation of Feige 66 for Hβ (blue side; left panel), and Hα (red side; right panel). The photon counts measured at each pixel along the slit are normalized by the peak value (blue dots). Two Gaussian functions (red lines) are used for the best-fit PSF model (black line). The residuals are shown at the bottom of each panel (dashed line).

(A color version of this figure is available in the online journal.)

[N II] λ6548 ratio as 3.0, while we use a single Gaussian model for other emission lines. In this procedure, we measure the central wavelength and line dispersion and their uncertainties of each emission line simultaneously, in order to investigate the kinematics of nebular emission. We correct for the instrumental broadening by subtracting the instrumental resolution from the measured line dispersion in quadrature as generally practiced (e.g., Barth et al. 2002; Woo et al. 2004). In case of the [O III] λ5007 at +1.1 kpc aperture, the measured line dispersion (~2.4 Å) is comparable to the instrumental resolution (~2.5 Å for the blue side); hence, we did not correct for the instrumental resolution and the measured line dispersion of [O III] should be taken as an upper limit.

Systematic uncertainty of the radial velocity comes from the uncertainty of wavelength calibration, which was estimated as~0.2 Å by adopting the standard deviation of arc or sky line wavelengths with respect to the wavelength solution. The measurement errors of the line velocity derived from the Monte Carlo realization are less than or comparable to the systematic error in most cases. Hence, we added both errors in quadrature to obtain the final uncertainty of each emission-line velocity. For the line dispersion measurements, on the other hand, we only consider the measurement error derived from the Monte Carlo realization.

3.3. Point-spread Function

A precise measurement of a PSF is an important task to examine whether the LINER-like features are originated from an extended or nuclear region. To measure the PSF we utilize the spectrophotometric stars observed right before and after observing the target galaxy. Using photon counts of each pixel from standard star observations, we obtained the spatial profile of PSF at each wavelength range, which corresponds to the spectral range of each emission lines. For each emission-line region, we performed a median combine by using 10 pixels along the dispersion direction, then we constructed a model PSF by fitting the observed PSF with multi-Gaussian functions, resulting in one PSF for each emission line.

Figure 5 illustrates the PSF model based on the spatial distribution of a standard star Feige 66. Note that the spatial distribution is slightly extended than a single Gaussian. Thus, we used two Gaussian components for the best PSF model. In the Hβ region (Figure 5 left), we used FWHM 4″.91 and 1″.08,

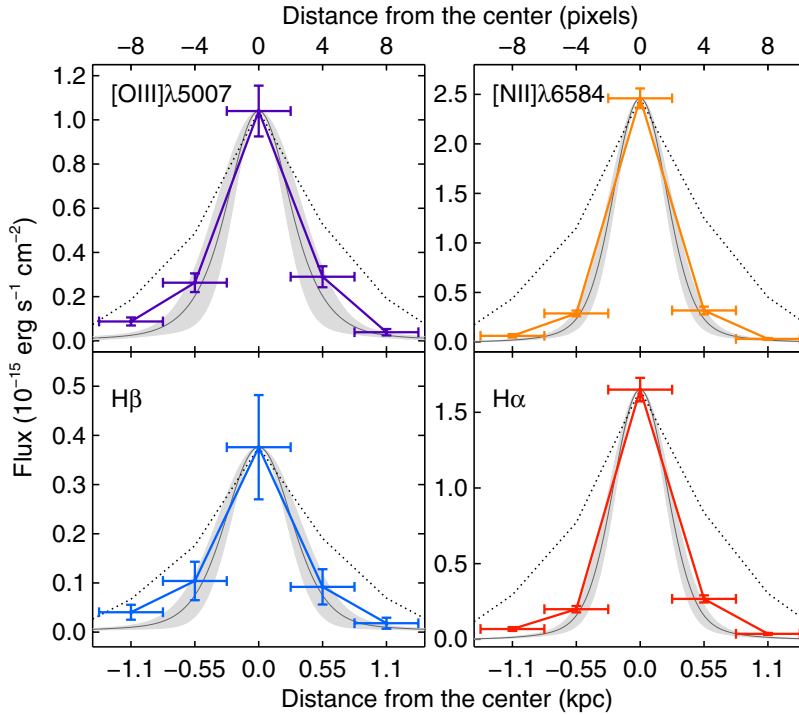wavelength range we used also contains the other emission lines, such as [S II], [O I], that are typically used in AGN diagnostics. However, we could not use those lines since the [S II] λλ 6716, 6731 lines fall in the atmospheric absorption *B* band and the [O I] λ6300 line is too weak to properly measure line flux. In Figure 4, we present the emission lines after subtracting stellar component and the best-fit single Gaussian models.

We use the Monte Carlo technique to measure the mean strength, wavelength, and dispersion, and estimate their uncertainties for each emission line simultaneously. First of all, we take a standard deviation of the continuum fitting residuals within ~±100 Å range from the center of each emission line as a proxy for systematic uncertainties, which is larger than the measurement uncertainties in the emission-line fitting process. Thus, the uncertainties adopted in the following simulations should be considered as upper limits. Then, we generate a thousand simulated spectra using the random values at each pixel, which follow a normal distribution with the systematic uncertainty as a standard deviation, and add them to the emission lines. For each simulated spectrum, we measure line fluxes using a Gaussian model fitting method as follows. For the Hα+[N II] region, we use triple Gaussian models by constraining the [N II] λ6584-to-

Figure 6. Spatial profiles of emission-line flux: [O III] λ5007 (top left), Hβ (bottom left), [N II] λ6584 (top right), and Hα (bottom right). Thick solid lines indicate the profile of each emission line, and vertical error bars indicate a standard deviation of the measured fluxes from the Monte Carlo realization, while horizontal error bars represent the size of aperture for each emission-line flux. Dotted lines are normalized stellar continuum flux at 5100 Å (F_{5100}). Gray shade for each panel indicates that the minimum-to-maximum PSF range of the observation. We also plot the mean of both PSFs along the slit with a thin solid line over the gray shade.

(A color version of this figure is available in the online journal.)

respectively, for weak and strong Gaussian components with the peak ratio of weak to strong components as 0.03 while in the Hα region (Figure 5 right) FWHM was 4″.91 and 1″.08, respectively, for weak and strong Gaussian components with the peak ratio of 0.06.

4. RESULTS

In this section, we present the results of spatial profiles of emission-line flux and kinematic analysis for emission-line gas and stellar component, and suggest the most probable ionizing sources for the observed LINER features, and possible explanations for the observed kinematics.

4.1. Spatial Profiles of Emission-line Flux

To examine whether the emission-line region is spatially extended, we investigate the radial distribution of each emission line by comparing the spatial profiles of emission lines with that of stellar component and the PSF determined in Section 3.3. Figure 6 presents the spatial profiles of the emission-line flux for [O III] λ5007, Hβ, [N II] λ6584, and Hα along the slit. We overlay the PSF determined in Section 3.3, after normalizing it to the emission-line flux at the center. Since the exact PSF at the time of exposure on the galaxy is not known, we assume the true PSF size is between the maximum and minimum PSF sizes of spectrophotometric stars as determined in Section 3.3, as plotted with black solid lines and gray shades.

We find that the spatial profiles of emission-line flux are slightly more extended than, but comparable to, the PSFs indicating that the emission-line gas is centrally concentrated. At −1.1 kpc, there is a noticeable excess of emission-line fluxes compared to the PSF, suggesting that the emission-line region

is slightly more extended than a point source. We compare the spatial profiles of emission-line region and stellar component, to investigate a physical link between stars and ionizing sources of the emission lines. In Figure 6, the spatial profile of stellar continuum flux at 5100 Å (F_{5100}) is presented after normalizing it to each emission-line flux at the center. Compared to the spatial distribution of stellar component, the emission-line region is centrally concentrated, implying that old stellar population may not be a primary ionizing source of the LINER feature. Unless old stellar population is concentrated at the galaxy center, there seems no direct physical link between the emission-line gas and old stars.

We note that the spatial profiles of the emission-line flux are asymmetric, while that of stellar continuum flux is symmetric. In Figure 6, for example, the line fluxes of [O III] λ5007 and Hβ at −1.1 kpc aperture are a factor of two larger than those of the same emission lines at +1.1 kpc aperture (see also Figure 4). Such asymmetric spatial profiles of the emission lines further suggest that ionizing source may not be physically linked to old stellar component.

We investigate whether the distribution of young stellar population is asymmetric by measuring the 4000 Å break index $D_n(4000)$ as defined by Balogh et al. (1999) since $D_n(4000)$ is an indicator of the presence of young stars. The $D_n(4000)$ indices measured from −1.1 kpc to 1.1 kpc apertures are, respectively, [1.81, 1.86, 1.95, 1.87, 1.80] with measurement error less than 0.01, showing that old stellar population is dominant for all aperture but with a frost of young stellar population. The symmetric trend of the $D_n(4000)$ indicates that the distribution of young stellar population is also symmetric, further implying that ionizing source is not primarily linked to both old and young stellar populations.
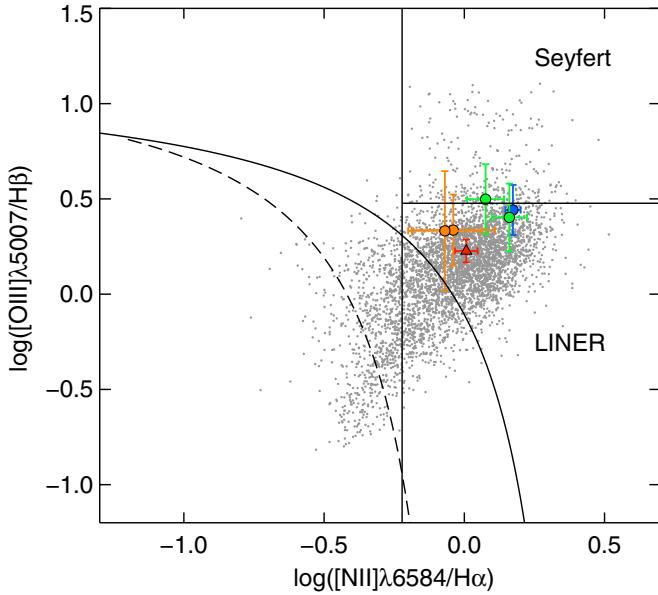
Figure 7. AGN diagnostics based on the emission-line ratios for each aperture. Compared to the emission-line ratio obtained from the SDSS integrated spectrum (red dot), the emission-line ratios measured from spatially resolved spectra are shown for the galaxy center (blue), ±0.55 kpc (green), and ±1.1 kpc (orange), respectively. SDSS early-type galaxies described in Section 2.1 are plotted for comparison (gray dots). Dashed and solid curved lines indicate empirical and theoretical demarcation lines between star-forming and AGN-host galaxies, respectively (Kauffmann et al. 2003; Kewley et al. 2001). Horizontal and vertical solid lines are demarcation lines for Seyfert and LINER galaxies, indicating [O III] $\lambda5007$/Hβ = 3.0 and [N II] $\lambda6584$/Hα = 0.6, respectively (Kauffmann et al. 2003).

(A color version of this figure is available in the online journal.)

Figure 7 presents the AGN diagnostic diagram with flux ratios of [N II] $\lambda6584$ to Hα and [O III] $\lambda5007$ to Hβ measured at each aperture. We find that both line ratios tend to decrease from the central to outer (±1.1 kpc) apertures, implying that ionizing power varies as a function of the radial distance from the center. However, we note that the decrease of the [N II]/Hα flux ratio can be interpreted as the decrease of gas density and/or metallicity. To compare with the flux ratio measured from fiber observations, we plot the fiber-integrated emission-line ratios based on the SDSS spectrum. The integrated emission-line ratios are ~0.2 dex lower than those measured at the center, implying that the emission-line ratios based on the fiber-integrated spectra can be significantly underestimated compared to the central emission-line ratios.

4.2. Kinematics of Emission-line Gas

Comparing the kinematic properties of emission-line gas and stellar component can provide an important clue on the nature of the ionizing sources. In Figure 8, we present the line-of-sight velocities and velocity dispersions of each emission line and stellar component measured at five different locations along the slit. The line-of-sight velocity measured from stellar lines at the galaxy center is 7218 ± 2 km s^{-1}, which is consistent within the error with the SDSS redshift $z = 0.0241 \pm 0.0002$, corresponding to 7225 ± 60 km s^{-1}. By adopting the line-of-sight velocity measured from stellar component at the galaxy center as a zero point, we present the relative velocities of gas and stellar components. For emission lines, we adopt the air wavelength provided by Morton (1991) as a rest-frame wavelength to calculate the radial velocity of each emission line.
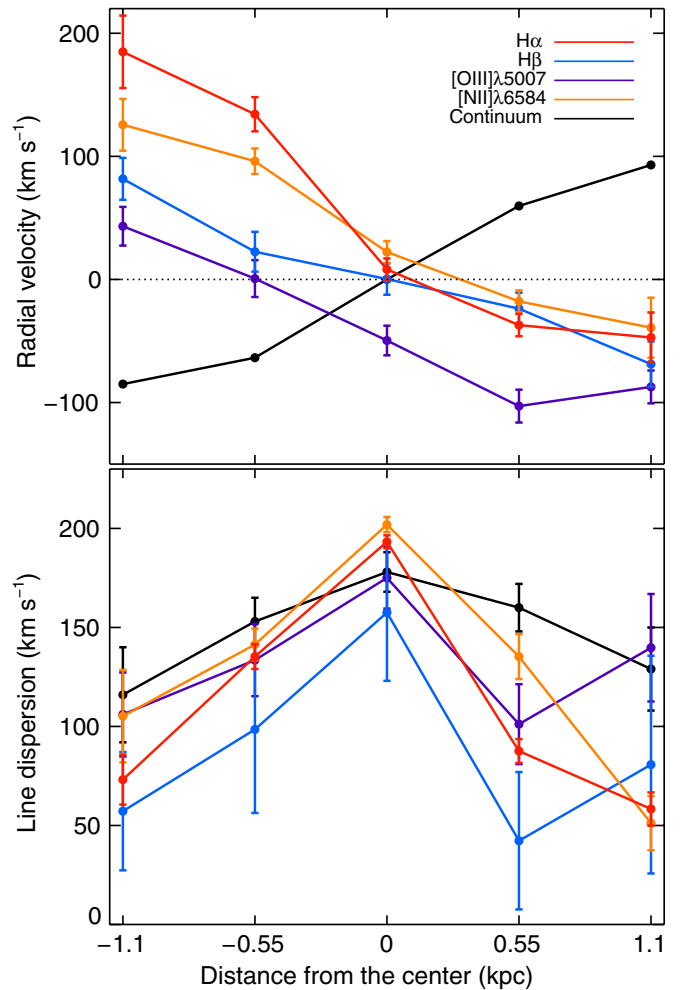

Figure 8. Kinematic properties of the nebular emission and stellar continuum along the slit. The upper and bottom panels show the spatial profiles of the line-of-sight velocity and velocity dispersion, respectively. Adopted color codes are the same as in Figure 6. The uncertainties of the line velocities are estimated by adding systematic and measurement errors in quadrature (upper panel) while the error bars of line dispersion indicate the measurement errors (lower panel).

(A color version of this figure is available in the online journal.)

We find several characteristics of the emission-line gas and stellar component. First, there is a rotating stellar component with a line-of-sight velocity of ~±90 km s^{-1} at ~±1 kpc. Since the old stars are dominant in the luminosity-weighted galaxy spectra, the rotation is mainly represented by old stellar population. It is not unusual to find a rotating stellar component among early-type galaxies (e.g., Emsellem et al. 2007, 2011). For example, based on the integral field spectroscopic observations of a sample of 48 nearby early-type galaxies, Emsellem et al. (2007) reported that all early-type galaxies in their sample were either slow or fast rotator.

Second, emission-line gas is counter-rotating with respect to stellar component, indicating that gas and stellar component are kinematically decoupled. The dynamical detachment implies that emission-line region may not be directly related to stellar component, although we cannot rule out the stellar component as ionizing sources solely based on the dynamical decoupling.

Third, [O III] $\lambda5007$ emission line is significantly blueshifted with respect to stellar component, by -56 ± 12 km s^{-1} at the center, while other emission lines do not show clear velocity offset. An artifact due to a misaligned slit position may cause the

velocity offset (Comerford et al. 2009); however, the detected offset is not an artifact since the radial velocities of all other emission lines except [O III] $\lambda 5007$ are consistent with the reference velocity of stellar lines.

While the velocity offset of emission-line gas at the center of LINER galaxies has not been reported,[10] it is rather common in Seyfert galaxies. Investigating [O III] $\lambda 5007$ line for 65 local Seyfert galaxies, for example, Crenshaw et al. (2010) summarized that 6% of the Seyferts display redshifted velocity offset with $\Delta v \geqslant +50\,\mathrm{km\,s^{-1}}$, and 35% display blueshifted offset with $\Delta v \leqslant -50\,\mathrm{km\,s^{-1}}$. They provided a physical interpretation that the offset is due to the combined effect of gas outflow of ionized gas in the NLR and dust extinction in the inner stellar disk (see Figure 7 of Crenshaw et al. 2010). Although this scenario was developed for Seyfert galaxies, it is a viable solution for the velocity offset detected in the LINER galaxy, assuming that as a minor version of Seyfert galaxies, LINER galaxies also have mass outflow at the center (e.g., Kewley et al. 2006). Compared to other scenarios, e.g., infalling small galaxy to the center of an AGN-host galaxy (Heckman et al. 2009) or alignment of two AGNs (Shields et al. 2009), the outflow scenario provides a simpler explanation for the velocity offset of emission-line gas. Following the outflow scenario, it is probable that we only detected the [O III] velocity offset because [O III] ionization region is closer to the accretion disk, hence, more affected by an outflow (e.g., Komossa et al. 2008).

Counter-rotating gas disks are often found in nearby early-type galaxies based on longslit spectroscopy, e.g., NGC 4621 (Bender 1990), NGC 4450 (Rubin et al. 1992), and early-type galaxies of recent IFU surveys (e.g., Emsellem et al. 2007, 2011). The observed velocity offset of [O III] may be explained by that outflow gas is mixed with the counter-rotating disk, producing the velocity offset with respect to stellar component and the rotation at the same time. It seems that spatial distribution and dynamics of NLR gas in the LINER galaxy is rather complex as similarly found in other local LINER galaxies (Pogge et al. 2000).

We investigate whether the LINER has an appropriate accretion rate to generate an outflow. Based on the empirical relationship between the mass of supermassive black hole (M_{BH}) and stellar velocity dispersion (Gültekin et al. 2009), we estimate black hole mass as $\approx 1.1 \times 10^8\,M_\odot$ from the stellar velocity dispersion $\sim 178 \pm 10\,\mathrm{km\,s^{-1}}$ measured at the galaxy center. To measure bolometric luminosity (L_{bol}) we use the narrow Hα luminosity. Although it is more difficult to measure the L_{bol} of Type 2 AGNs than that of Type 1 AGNs due to the lack of broad emission lines, the narrow Hα line can be used as a proxy for the broad emission lines and the bolometric luminosity (Ho 2009). By adopting the bolometric correction factor $C_{\mathrm{H}\alpha} \sim 100$ (Ho 2009), we obtain $L_{\mathrm{bol}} \approx 6.0 \times 10^{40}\,\mathrm{erg\,s^{-1}}$ from the narrow Hα line luminosity at the galaxy center. Combining the M_{BH} and L_{bol} estimates, we derive the Eddington ratio as $\sim 4.2 \times 10^{-6}$, which is similar to the Eddington ratios of nearby LINER galaxies (Ho 2009). In such a low Eddington ratio regime, AGN outflow is unlikely to be present due to the low radiative pressure compared to the gravitational force (e.g., Raimundo et al. 2010).

In contrast to the theoretical expectations, however, several observational studies reported LINER galaxies with a distinguishable outflow (e.g., Walsh et al. 2008; Masegosa et al. 2011).

For example, Walsh et al. (2008) presented clear evidence for nuclear outflow of several nearby LINER galaxies. In addition, NLR morphologies of nearby LINER galaxies are disturbed (Pogge et al. 2000), implying that the disturbed morphology is closely related to the outflow from the center (Masegosa et al. 2011). Although it is still puzzling how LINERs with low Eddington ratios can exhibit an outflow, the observed kinematics of the emission-line gas in the LINER galaxy seems to be connected with an outflow from the central AGN.

5. DISCUSSIONS AND SUMMARY

As a pilot study for investigating the nature of ionizing sources in LINERs, we observed a LINER early-type galaxy, SDSS J091628.05+420818.7, with Keck/LRIS to obtain spatially resolved spectra. By comparing with the PSF of the observations, we find that the emission-line region is slightly extended, but comparable to the seeing size, indicating that emission-line gas is centrally concentrated and triggered by a central source. We find that emission-line gas is counter-rotating with respect to stellar component and a significant radial velocity offset of [O III] $\lambda 5007$ line.

We suggest a scenario that gas outflow in the NLR is ionized by a central source, presumably an active black hole, and mixed with gas in the counter-rotating disk. Though it is still difficult to disentangle the gas origin in this work, the gas is unlikely to be ionized and originated from the evolved stars from the old stellar population, since the gas is kinematically decoupled with the old stellar population. The counter-rotating gas may have external (e.g., Rubin et al. 1992) or internal origins such as evolved stars (e.g., Ho et al. 2009), and the gas may be causally linked with the existence of a young stellar population. We cannot exclude the possibility that the young stars could be an ionizing source, but the contribution would be much weaker compared to that of AGNs as the spatially concentrated profiles of emission-line flux indicate.

Although some LINER galaxies may show an extended emission-line region, it is still possible that an active black hole is hidden in the integrated spectra. Thus, we cannot simply exclude the LINER galaxies identified in SDSS from the AGN population in the local universe. Detailed studies based on spatially resolved spectra are necessary to reveal the true nature of the ionizing source of LINERs.

---

[10] Although Barth et al. (2008) reported that a radial velocity offset in one of LINER nuclei in NGC 3341, it is due to remote LINER nucleus from the center.

was supported by Subaru Telescope which is operated by the National Astronomical Observatory of Japan, as a Subaru/Keck time exchange program.

REFERENCES

Abazajian, K. N., Adelman-McCarthy, J. K., Ageros, M. A., et al. 2009, ApJS, 182, 543
Annibali, F., Bressan, A., Rampazzo, R., et al. 2010, A&A, 519, 40
Baldwin, J. A., Phillips, M. M., & Terlevich, R. 1981, PASP, 93, 5
Balogh, M. L., Morris, S. L., Yee, H. K. C., Carlberg, R. G., & Ellingson, E. 1999, ApJ, 527, 54
Barth, A. J., Bentz, M. C., Greene, J. E., & Ho, L. C. 2008, ApJ, 683, L119
Barth, A. J., Ho, L. C., & Sargent, W. L. W. 2002, AJ, 124, 2607
Becker, R. H., White, R. L., & Helfand, D. J. 1995, ApJ, 450, 559
Bender, R. 1990, A&A, 229, 441
Binette, L., Magris, C. G., Stasińska, G., & Bruzual, A. G. 1994, A&A, 292, 13
Bower, R. G., Benson, A. J., Malbon, R., et al. 2006, MNRAS, 370, 645
Capetti, A., & Baldi, R. D. 2011, A&A, 529, 126
Cappellari, M., & Emsellem, E. 2004, PASP, 116, 138
Cappellari, M., Emsellem, E., Krajnović, D., et al. 2011, MNRAS, 413, 813
Cid Fernandes, R., Stasińska, G., Mateus, A., & Vale Asari, N. 2011, MNRAS, 413, 1687
Comerford, J. M., Gerke, B. F., Newman, J. A., et al. 2009, ApJ, 698, 956
Crenshaw, D. M., Schmitt, H. R., Kraemer, S. B., Mushotzky, R. F., & Dunn, J. P. 2010, ApJ, 708, 419
Croton, D. J., Springel, V., White, S. D. M., et al. 2006, MNRAS, 365, 11
Dopita, M. A., & Sutherland, R. S. 1995, ApJ, 455, 468
Emsellem, E., Cappellari, M., Krajnović, D., et al. 2007, MNRAS, 379, 401
Emsellem, E., Cappellari, M., Krajnović, D., et al. 2011, MNRAS, 414, 888
Falcón-Barroso, J., Peletier, R. F., Emsellem, E., et al. 2004, MNRAS, 350, 35
Ferrarese, L., & Merritt, D. 2000, ApJ, 539, L9
Filippenko, A. V. 1996, in ASP Conf. Ser. 103, The Physics of LINERs in View of Recent Observations, ed. M. Eracleous, A. Koratkar, C. Leitherer, & L. Ho (San Francisco, CA: ASP), 17
Gebhardt, K., Bender, R., Bower, G., et al. 2000, ApJ, 539, L13
Gültekin, K., Richstone, D. O., Gebhardt, K., et al. 2009, ApJ, 698, 198
Heckman, T. M. 1980, A&A, 87, 152
Heckman, T. M., Krolik, J. H., Moran, S. M., Schnittman, J., & Gezari, S. 2009, MNRAS, 398, L73
Ho, L. C. 2008, ARA&A, 46, 475
Ho, L. C. 2009, ApJ, 699, 626
Ho, L. C. 2009, ApJ, 699, 638
Ho, L. C., Filippenko, A. V., & Sargent, W. L. W. 1997, ApJ, 487, 568
Hopkins, P. F., Hernquist, L., Cox, T. J., et al. 2005, ApJ, 630, 705
Kauffmann, G., Heckman, T. M., Tremonti, C., et al. 2003, MNRAS, 346, 1055
Kaviraj, S., Schawinski, K., Devriendt, J. E. G., et al. 2007, ApJS, 173, 619

Keel, W. C. 1983, ApJ, 268, 632
Kewley, L. J., Dopita, M. A., Sutherland, R. S., Heisler, C. A., & Trevena, J. 2001, ApJ, 556, 121
Kewley, L. J., Groves, B., Kauffmann, G., & Heckman, T. 2006, MNRAS, 372, 961
Kroupa, P. 2001, MNRAS, 322, 231
Komossa, S., Xu, D., Zhou, H., Storchi-Bergmann, T., & Binette, L. 2008, ApJ, 680, 926
Maoz, D., Nagar, N. M., Falcke, H., & Wilson, A. S. 2005, ApJ, 625, 699
Markwardt, C. B. 2009, in ASP Conf. Ser. 411, Astronomical Data Analysis Software and Systems XVIII, ed. D. A. Bohlender, D. Durand, & P. Dowler (San Francisco, CA: ASP), 251
Martin, D. C., Fanson, J., Schiminovich, D., et al. 2005, ApJ, 619, L1
Masegosa, J., Márquez, I., Ramirez, A., & González-Martín, O. 2011, A&A, 527, 23
McGill, K. L., Woo, J.-H., Treu, T., & Malkan, M. A. 2008, ApJ, 673, 703
Monreal-Ibero, A., Arribas, S., & Colina, L. 2006, ApJ, 637, 138
Moré, J. 1978, in Numerical Analysis, Vol. 630, ed. G. A. Watson (Berlin: Springer), 105
Morton, D. C. 1991, ApJS, 77, 119
Oke, J. B. 1990, AJ, 99, 1621
Oke, J. B., Cohen, J. G., Carr, M., et al. 1995, PASP, 107, 375
Park, C., & Choi, Y.-Y. 2005, ApJ, 635, L29
Pogge, R. W., Maoz, D., Ho, L. C., & Eracleous, M. 2000, ApJ, 532, 323
Raimundo, S. I., Fabian, A. C., Bauer, F. E., et al. 2010, MNRAS, 408, 1714
Rich, J. A., Dopita, M. A., Kewley, L. J., & Rupke, D. S. N. 2010, ApJ, 721, 505
Rockosi, C., Stover, R., Kibrick, R., et al. 2010, Proc. SPIE, 7735, 77350R
Rubin, V. C., Graham, J. A., & Kenney, J. D. P. 1992, ApJ, 394, L9
Sánchez-Blázquez, P., Peletier, R. F., Jiménez-Vicente, J., et al. 2006, MNRAS, 371, 703
Sarzi, M., Shields, J. C., Schawinski, K., et al. 2010, MNRAS, 402, 2187
Shields, G. A., Bonning, E. W., & Saliander, S. 2009, ApJ, 696, 1367
Springel, V., Di Matteo, T., & Hernquist, L. 2005, ApJ, 620, 795
Stanghellini, L., & Renzini, A. 2000, ApJ, 542, 308
Stasińska, G., Vale Asari, N., Cid Fernandes, R., et al. 2008, MNRAS, 391, L29
Taniguchi, Y., Shioya, Y., & Murayama, T. 2000, AJ, 120, 1265
van Dokkum, P. G. 2001, PASP, 113, 1420
Veilleux, S., Kim, D.-C., Sanders, D. B., Mazzarella, J. M., & Soifer, B. T. 1995, ApJS, 98, 171
Walsh, J. L., Barth, A. J., Ho, L. C., et al. 2008, AJ, 136, 1677
Woo, J.-H., Treu, T., Barth, A. J., et al. 2010, ApJ, 716, 269
Woo, J.-H., Treu, T., Malkan, M. A., & Blandford, R. D. 2006, ApJ, 645, 900
Woo, J.-H., Urry, C. M., Lira, P., van der Marel, R. P., & Maza, J. 2004, ApJ, 617, 903
Yan, R., & Blanton, M. R. 2012, ApJ, 747, 61
York, D. G., Adelman, J., Anderson, J. E., Jr., et al. 2000, AJ, 120, 1579